Excited-state trions in two-dimensional materials

Jun Yan
Department of Physics, University of Massachusetts, Amherst, Massachusetts 01003, USA

Kalman Varga*
Department of Physics and Astronomy, Vanderbilt University, Nashville, Tennessee 37235, USA

(Received 7 May 2020; revised manuscript received 10 June 2020; accepted 12 June 2020; published 22 June 2020)

Using the complex scaling and the stabilization method combined with the stochastic variational approach, we have shown that there are narrow resonance states in two-dimensional three particle systems of electrons and holes interacting via a screened Coulomb interaction. These resonances are loosely bound systems of excited state excitons with a third particle circling around them. Recent experimental studies of excited state trions might be explained and identified by these resonant states.

DOI: 10.1103/PhysRevB.101.235435

I. INTRODUCTION

Monolayers of transition metal dichalcogenides (TMD) are chemically and mechanically stable making them ideal systems for studying physics in two dimensions (2D). The reduced dimensionality leads to a notably strong Coulomb interaction between charge carriers [1]. This enhanced interaction, in turn, leads to the formation of tightly bound excitons [2–6], charged excitons (trions) [7–11], and biexcitons [12–21].

Theoretical studies [22–40] played an important role in predicting the stability and properties of these electron-hole complexes. Energies of excitons can be calculated by solving the Bethe-Salpeter equation (BSE) in the quasiparticle band structure framework [25,26,41]. The effective mass approach with 2D interaction potential has also been successfully used to calculate binding energies [22,23,27–32,35,37,39,42–44] in good agreement with the BSE approach and the experimental results. In the effective mass models the excitonic systems are considered to be few particle systems, e.g., the trion is the bound state of three particles. Other interpretations also exist where trions are described as excitons dressed by interactions with a Fermi sea of excess carriers [38].

Recent experimental studies have shown the existence of excited state trions in TMDs [11,45]. This is somewhat surprising, because the trion has no known bound excited state. In fact neither the H^- (p, e^-, e^-) nor the Ps^- (e^+, e^-, e^-) ion has bound states in two or three dimensions [46–49]. The H^- and Ps^- ion, however, has many resonant states in three dimensions [50–52].

In this paper we will investigate the existence of these resonant states in 2D materials. Unlike bound states, the resonances have complex energies and spatially extended non-L^2 wave functions. Conventional variational approaches based on square integrable real basis functions cannot be directly used to calculate these resonant excited states. We will use two distinct approaches, the real stabilization method [53], and the complex scaling (CS) [54,55] approach to finding the resonant states. Both of these approaches need a flexible variational basis. We will use the stochastic variational method (SVM) [56] with explicitly correlated Gaussians (ECG) [46] to generate basis states.

The stabilization method (SM) [53] is based on the observation that a sufficiently large-square integrable basis set yields good approximations to the inner part of the exact resonance wave functions at energies equal to the eigenvalues of the Hamiltonian matrix. Eigenvalues belonging to resonant states remain stable when the basis dimension is increased. The degree of stability of the eigenvalues approximating the energy of the resonance is proportional to the width of the resonance. The complex energy of the resonance state can be extracted from the change in the stable eigenvalue as the size of the basis increases.

In the complex scaling method [54,55], the coordinates are rotated into the complex plane and resonant wave function becomes square integrable and can be expanded in terms of real basis functions. The trajectory of the eigenenergies of the Hamiltonian as a function of rotation angle is very different for bound, scattering, and resonance states. The energy and width of the resonances can be determined from the converged position of the complex eigenvalues.

The stochastic variational method will be used to generate a square-integrable basis using explicitly correlated Gaussians [46] for the CS and SM calculations. The SVM has been previously shown to achieve accuracy of up to 8–10 digits when describing the binding energies of similar systems such as H_2, H_2^+, and the positronium molecule (Ps_2) [48,57]. This method has proven to be well suited for describing the binding energies of excitonic structures ranging from the two-body exciton to five-body exciton-trion systems [30,47,49]. Previously, we have shown that this method yields values that agree with other calculations and experimental findings for the binding energies of excitons and trions in TMDs [30,31].

*kalman.varga@vanderbilt.edu

II. FORMALISM

A. Hamiltonian and basis functions

The nonrelativistic Hamiltonian of an excitonic few-particle system is given by

$$H = -\sum_{i=1}^{N} \frac{\hbar^2}{2m_i}\nabla_i^2 + \sum_{i<j}^{N} V(r_{ij}), \tag{1}$$

where $r_{ij} = |\mathbf{r}_i - \mathbf{r}_j|$, and $\mathbf{r}_i$, m_i, are the 2D position vector and the effective mass of the particle.

In the case of an excitonic system in 2D, the interaction potential $V(r_{ij})$ is given by the 2D screened electrostatic interaction potential derived by Keldysh [58]

$$V(r_{ij}) = \frac{q_i q_j}{\kappa r_0} V_{2D}\left(\frac{r_{ij}}{r_0}\right), \tag{2}$$

where

$$V_{2D}(r) = \frac{\pi}{2}[H_0(r) - Y_0(r)]. \tag{3}$$

This potential has been adopted in most of the calculations. Alternative potentials have also been proposed [59] to better describe three atomic sheets that compose a monolayer TMD. In the screened potential q_i is the charge of the ith particle, and r_0 is the screening length indicative of the medium. κ is the average environmental dielectric constant. H_0 and Y_0 are the Struve function and Bessel function of the second kind, respectively.

The nonlocal macroscopic screening, inherent to 2D systems, distinguishes this potential from its 3D Coulombic counterpart [25]. The length scale of this screening is determined by the 2D layer polarizability χ_{2D} as $r_0 = 2\pi\chi_{2D}/\kappa$. In the limit of very strong screening ($r_0 \to \infty$), the potential exhibits a logarithmic divergence, while in the limit of small screening length ($r_0 \to 0$), $V(r_{ij})$ approaches the usual $1/r$ behavior of the Coulomb potential.

The variational method is used to calculate the energy of the system. As a trial function we choose a 2D form of the correlated Gaussians [46,56]:

$$\exp -\frac{1}{2}\sum_{i,j=1}^{N} A_{ij}\mathbf{r}_i \cdot \mathbf{r}_j, \tag{4}$$

where A_{ij} are the nonlinear parameters. The above form of the CG belongs to $M = 0$. To allow for $M \neq 0$ states, we multiply the basis by

$$\prod_{i=1}^{N} \xi_{m_i}(\mathbf{r}_i), \tag{5}$$

where

$$\xi_m(\boldsymbol{\rho}) = (x + iy)^m. \tag{6}$$

Thus our nonrestrictive CG function reads as

$$\Phi_A(\mathbf{r}) = \mathcal{A}\left\{\left(\prod_{i=1}^{N}\xi_{m_i}(\mathbf{r}_i)\right)\exp\left\{-\frac{1}{2}\sum_{i,j=1}^{N} A_{ij}\mathbf{r}_i\cdot\mathbf{r}_j\right\}\right\}, \tag{7}$$

where $M = m_1 + m_2 + \cdots + m_N$, m_i are integers, and $\mathcal{A}$ is an antisymmetrizing operator. This function is coupled with the spin function χ_{SM_S} to form the trial function. The nonlinear parameters are optimized using the stochastic variational method [46,56].

ECG are very popular in atomic physics and quantum chemistry [46]. The main advantages of ECG bases are (1) their matrix elements are analytically available for a general N-particle system, (2) they are flexible enough to approximate rapidly changing functions, and (3) the permutation symmetry can be easily imposed.

Reference [46] provides a thorough review of the applications of the ECG basis in various problems. Benchmark tests presented for atoms with $N = 2 - 5$ electrons show that the ECG basis can produce up to ten digit accuracy for 2–3 electron atoms. The ECG basis has also proven to be very accurate in calculating weakly bound states. A series of positronic atoms have been predicted using the stochastic variational method with an ECG basis [48,60]. The binding energy of these systems [46] ranges from 0.001 to 0.04 a.u. (1 a.u. is 27.211 eV) with weakly bound diffuse structures similar to those studied here.

B. Complex scaling

The complex scaling method was originally proposed by Aguilar, Balslev, and Combes [61,62]. The CS is introduced by a transformation $U(\theta)$ with a scaling angle θ for the radial coordinate $\mathbf{r}$

$$U(\theta)\,\mathbf{r}\,U^{-1}(\theta) = \mathbf{r}\,e^{i\theta}, \tag{8}$$

where $U(\theta)U^{-1}(\theta) = 1$. The Schrödinger equation, $H\Psi = E\Psi$, is transformed as

$$H^\theta\Psi^\theta = E^\theta\Psi^\theta, \tag{9}$$

$$H^\theta = U(\theta)HU^{-1}(\theta), \tag{10}$$

To solve Eq. (10), the wave functions $\Psi_k^\theta(\mathbf{r})$ are expanded in terms of ECG basis functions:

$$\Psi_k^\theta(\mathbf{r}) = \sum_{i=1}^{K} c_{ik}(\theta)\,\Phi_{A_i}(\mathbf{r}), \tag{11}$$

leading to the generalized complex eigenvalue problem

$$\sum_{j=1}^{K} H_{ij}^\theta\, c_{jk}(\theta) = \epsilon_k^\theta \sum_{j=1}^{K} O_{ij} c_{jk}(\theta), \tag{12}$$

$$H_{ij}^\theta = \langle\Phi_{A_i}|H^\theta|\Phi_{A_j}\rangle, \tag{13}$$

$$O_{ij} = \langle\Phi_{A_i}|\Phi_{A_j}\rangle, \tag{14}$$

where H_{ij}^θ are the matrix elements of the complex-scaled Hamiltonian and O_{ij} is the overlap of the basis functions. In the case of Coulomb interactions the CS Hamiltonian is particularly simple:

$$H_{ij}^\theta = \mathrm{e}^{-2\theta}T_{ij} + \mathrm{e}^{-\theta}V_{ij}, \tag{15}$$

where T_{ij} and V_{ij} are the kinetic and potential energy matrices of the ECG basis functions.

The ABC theorem of Aguilar, Combes, and Balslev [61,62] describes the properties of the of the CS eigenstates:

(a) Energies of bound states are invariant with respect to the rotation angle.

(b) Resonance states can be described by square-integrable functions.

(c) The continuum spectra start at the threshold energies corresponding to the decays of the system into subsystems. The spectra are rotated clockwise by 2θ from the positive real energy axis.

In the CS method the resonances are determined by finding the position where the complex eigenvalues are stabilized with respect to the rotation angle:

$$\left.\frac{\partial E}{\partial \theta}\right|_{\theta=\theta_{opt}} = \min. \tag{16}$$

Once the position of resonance is determined, the resonance energy (E_r) and total width (Γ) are given by

$$E_r - i\tfrac{1}{2}\Gamma. \tag{17}$$

C. Stabilization method

In this method we also use a variational ECG basis ansatz

$$\Psi_k^{(K)}(\mathbf{r}) = \sum_{i=1}^{K} c_{ik}\, \Phi_{A_i}(\mathbf{r}), \tag{18}$$

but now we use the dimension of the basis, K, as a parameter (expansion length). The corresponding generalized real eigenvalue problem reads as

$$\sum_{j=1}^{K} H_{kj}, c_{ji}(\theta) = \epsilon_i^{(K)} \sum_{j=1}^{K} O_{kj} c_{ji}(\theta), \tag{19}$$

$$H_{ij}^{\theta} = \langle \Phi_{A_i} | H | \Phi_{A_j} \rangle, \tag{20}$$

where $\epsilon_i^{(K)}$ is the variational estimate to the energy of the ith state of the system. In the following we will use E_i for the energy of the ith state dropping the basis dimension (K) if it is not important.

The simplest version of the stabilization method [53] is based on the Hylleraas-Undheim theorem [63,64]. The Hylleraas-Undheim theorem states that (i) comparing the variational energy estimates obtained with K trial wave functions and the estimate obtained by adding one additional orthonormalized trial wave function (increasing the basis dimension to $K+1$), one finds that the new energy estimates are interleaved with the old ones:

$$\epsilon_0^{(K+1)} \leqslant \epsilon_0^{(K)} \leqslant \epsilon_1^{(K+1)} \leqslant \epsilon_1^{(K)} \leqslant \ldots \epsilon_{K-1}^{(K+1)} \leqslant \epsilon_{K-1}^{(K)} \leqslant \epsilon_K^{(K+1)} \tag{21}$$

and (ii) the eigenvalues $\epsilon_i^{(K)}$ are upper limits to the corresponding excited states.

By increasing the basis dimension ("expansion length") the real part of the resonance energies becomes "stable". This stabilization occurs because the inner part of the wave function, at an energy in the resonant region, looks like the wave function of a bound state. The amplitude of the wave function in the asymptotic region is much smaller than the amplitude of its inner part. The inner part of the wave function is expanded in a set of discrete exponentially decaying functions, and then the Hamiltonian is diagonalized to yield the approximate resonance energies directly. Once the basis size is sufficiently large to represent the inner part, the energy of this state barely changes when more basis states are added because the asymptotic part is small and does not contribute to the energy. The energies of the nonresonant scattering wave functions, however, quickly change with the addition of basis states because their asymptotic parts are large.

There are many variants of the stabilization method, one can confine the wave functions with a potential and change the range of confinement, scale the coordinates or perturb the Hamiltonian in some way and find the stable states [65–69]. Most of these approaches can be used to extract the resonance widths as well [65–69].

D. Stochastic optimization

The basis parameters can be efficiently chosen via the stochastic variational method [56]. In this approach, the variational parameters A_{ij} of the ECG basis [see Eq. (7)] are randomly selected, and the parameters giving the lowest variational energy are retained as basis states. This procedure can be fine-tuned into an efficient optimization scheme as described in detail in Refs. [46,56].

In the present work, we found that the most efficient way to build a flexible basis is as follows:

(i) Optimize the ground state on a small ($K = 200$) basis selecting A_{ij} from a parameter space which confines the interparticle distances below 10 a.u.

(ii) Expand the basis by optimizing the lowest l states by minimizing

$$\sum_{i=1}^{l} (\epsilon_i^{(K)} - \epsilon)^2 \tag{22}$$

for each K by SVM. Here ϵ can be any number below the lowest eigenvalue. In this step A_{ij} is chosen to allow the interparticle distances to extend up to 100 a.u. This helps the description of the extended excited states.

E. Physical quantities

The following physical quantities will be used to describe the properties of the system and characterize the quality of the wave function. The pair correlation function is defined as

$$C_{pq}(\mathbf{r}) = \frac{2}{N(N-1)} \left\langle \Psi \left| \sum_{i<j}^{N} \delta(\mathbf{r}_i - \mathbf{r}_j - \mathbf{r}) \right| \Psi \right\rangle, \tag{23}$$

where p and q stand for electrons or holes, so C_{ee} is the electron-electron and C_{eh} is the electron-hole correlation function. Using $C_{pq}(r)$, the radial part of the correlation function, the powers of interparticle distances are given by

$$\langle r_{pq}^k \rangle = 2\pi \int_0^{\infty} r^k C_{pq}(r) r \, \mathrm{d}r. \tag{24}$$

F. Units

The effective electron and hole masses are denoted as

$$m_e^* = m_e m_0 \quad \text{and} \quad m_h^* = m_h m_0, \tag{25}$$

where m_0 is the mass of the electron. One can define an effective Bohr radius as

$$a^* = \frac{\hbar^2 \kappa}{\mu e^2} \tag{26}$$

where e is the electron's charge and

$$\mu = \frac{m_e^* m_h^*}{m_e^* + m_h^*} \tag{27}$$

is the reduced mass. This can be also written as

$$a^* = \frac{\kappa(1+\sigma)}{m_e} \frac{\hbar^2}{m_0 e^2} = \frac{\kappa(1+\sigma)}{m_e} a_0 \quad \sigma = \frac{m_e}{m_h}, \tag{28}$$

where $a_0 = \frac{\hbar^2}{m_0 e^2}$ is the hydrogenic Bohr radius ($a_0 = 5.29177$ Å). With this one can define

$$\tilde{r}_0 = r_0 / a^*, \tag{29}$$

the screening length normalized by the Bohr radius. Similarly, the effective Bohr energy

$$E^* = \frac{e^2}{\kappa a^*} = \frac{m_e}{\kappa^2(1+\sigma)} E_0, \tag{30}$$

where

$$E_0 = e^2 / a_0 \tag{31}$$

is the Hartree energy ($E_0 = 27.211$ eV).

The energy of the exciton and trion states only depends on $\tilde{r}_0$ and on the electron-hole mass ratio σ. In the following we will use atomic units. The energies of the exciton is analytically known for $\tilde{r}_0 = 0$ and $\sigma = 1$ [70]:

$$E^X_{ns} = -\frac{2}{(2n-1)^2}, \tag{32}$$

that is,-2 $-2/9$ and $-2/25$ a.u. for the $1s$, $2s$, and the $3s$ states, respectively.

To convert the results to eV and Å one has to multiply the energies by E^* and the distances by a^*. This is the same convention as used in Refs. [23,29,31]

III. RESULTS AND DISCUSSION

In this section, we will present the results of the calculations. The energies and distances are in atomic units (a.u.) unless noted otherwise. These units and their conversion to meV and Å are defined in Sec. II F. We will denote the relevant energy levels of trion by E_i, in particular E_0 is the energy of the bound ground state and E_i $(0 < i)$ is the energy of the ith excited resonance state.

A typical calculation starts with a SVM basis optimization for the trion. On a single processor (Intel i7-6850K CPU @3.6 GHz) that takes about 4 h for a basis size of $K = 1500$. The CS requires a complex diagonalization of the K dimensional complex Hamiltonian [Eq. (14)] for each θ values. In the SM approach one has to diagonalize the k dimensional real Hamiltonian for $k = 1, \ldots, K$. The SM and CS complement each other in the identification of resonances.

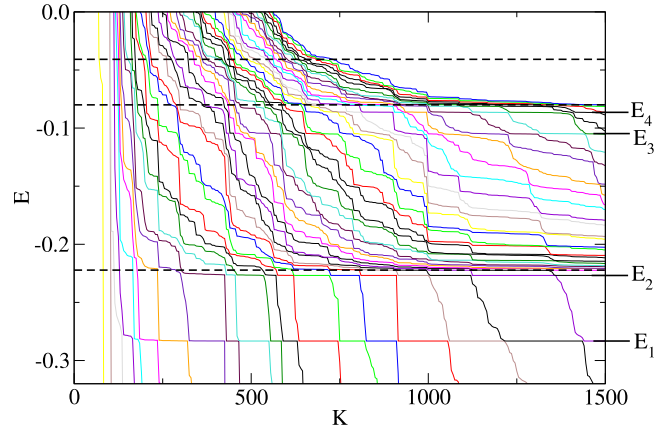

FIG. 1. Energy levels versus basis dimension. The four excited states energies (E_1, E_2, E_3 and E_4) are nicely stabilized as the energies are converging with the increased basis size. $\tilde{r}_0 = 0$ is used. The dashed lines show the $2s$, $3s$, and $4s$ exciton energies. The energies are in atomic units as defined in Sec. II F.

A. Spin singlet case

In this section we present the results for the spin singlet state of the trion.

1. Stabilization method ($\tilde{r}_0 = 0$)

Figure 1 shows the stabilization of the of the energy of trion resonance states. The lowest state, $E_1 = -0.28$ a.u., is stabilized at a small ($K = 200$) basis dimension and its energy remains unchanged after that. One can also see that at certain K values there are "avoided crossings" of the neighboring eigenvalues. The avoided crossing is a simple consequence of the Hylleraas-Undheim theorem. Let us assume that an isolated "stable" eigenvalue $\epsilon_j^{(K)}$ approximates E_1. With increasing K the next higher eigenvalue, $\epsilon_{j+1}^{(K)}$, decreases more rapidly than the stable eigenvalue $\epsilon_j^{(K)}$, and pushes $\epsilon_j^{(K)}$ away from E_1. At this point $\epsilon_{j+1}^{(K)}$ approaches E_1 and becomes the stable eigenvalue.

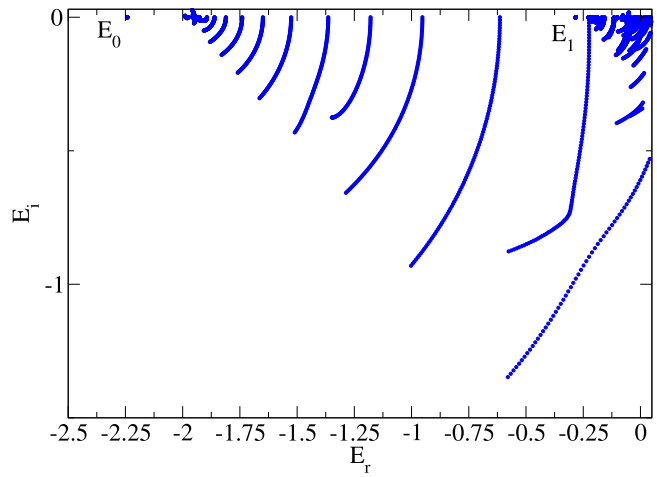

FIG. 2. Trajectories of the complex rotated energies. The energies are rotated from $\theta = 0$ to $\theta = 0.36$ (in rad) with a step size of $\Delta\theta = 0.004$ (in rad). $r_0 = 0$ is used. The energies are in atomic units as defined in Sec. II F.

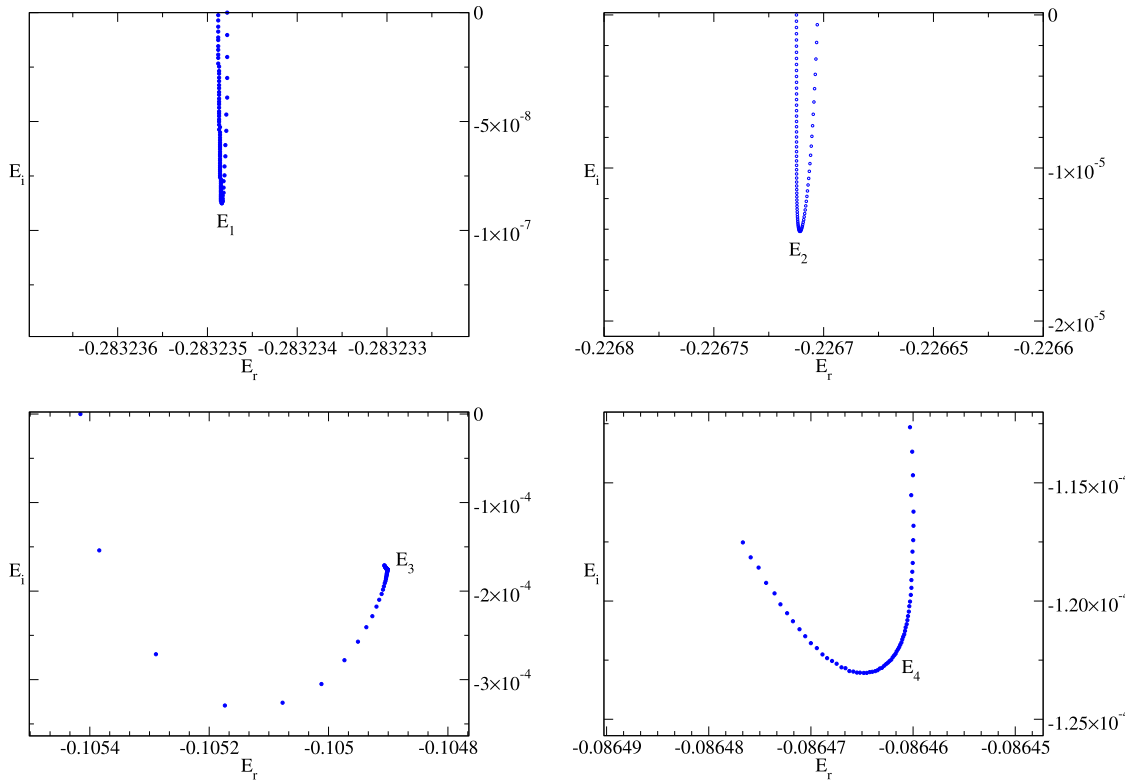

FIG. 3. Trajectories of the excited states of trion on the complex energy plane. The energies are rotated from $\theta = 0$ to $\theta = 0.1$ with a step size of $\Delta\theta = 0.004$ (in rad). $\tilde{r}_0 = 0$ is used. The energies are in atomic units as defined in Sec. II F.

The next resonance state, E_2 is slightly below the $2s$ threshold and it is also stable from about $K = 300$. There are at least two more stable resonant states, E_3 and E_4 below the $3s$ threshold. Figure 1 also shows that many states converge to the $2s$ and $3s$ thresholds from above. These states represent dissociation into $2s$ and $3s$ excitons and an electron.

All these resonance states are stabilized as a straight horizontal line which is a typical sign of a narrow resonance. This is confirmed by complex scaling as we will see later.

2. *Complex scaling method* ($\tilde{r}_0 = 0$)

As an illustration of the CS calculation, Fig. 2 shows the lowest 50 eigenvalues as the function of the rotation angle for a trion with $\sigma = 0$ and $\tilde{r}_0 = 0$. The basis dimension in all calculations is $K = 1500$. The ground state energy, E_0, is below the $1s$ exciton energy ($E^X_{1s} = -2$ a.u.), and the resonance state ($E_1 = -0.28$ a.u.) below the $2s$ exciton threshold ($E^X_{2s} = -2/9$ a.u.) remains stable. The continuum states rotated to the complex plane with an angle of 2θ. The first set of continuum states is rotated from the $1s$ threshold, the second starts at the $2s$ threshold.

By enlarging the CS calculation results in Fig. 2 around the resonant states, Fig. 3 shows 4 narrow resonance states in the complex energy plane. These are the same 4 states that are calculated by the stabilization method and shown in Fig. 1. These are all very narrow resonances.

Reference [51] also found four resonant states in the 3D case. The energies are different in 2D and 3D, but there are two resonances below the $2s$ threshold in both 2D and 3D. Reference [51] shows two resonances below the $3s$ threshold, our complex scaling approach shows at least three states.

Figure 4 shows the electron-electron (C_{ee}) and the electron-hole (C_{eh}) correlation functions for the ground state of trion. Due to the presence of the second electron the electron-hole correlation function is somewhat wider than that of the exciton. The electron-electron correlation function is pushed

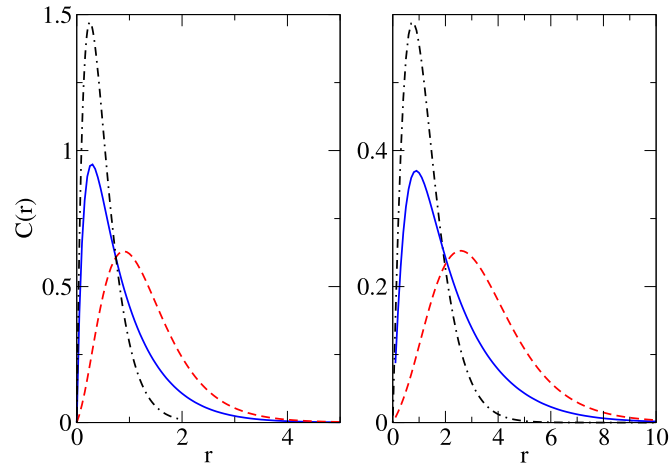

FIG. 4. Ground state correlation functions for $\tilde{r}_0 = 0$ (left) and $\tilde{r}_0 = 1$ (right). Electron-electron correlation, $C^t_{ee}(r)$ (dashed line), electron-hole correlation, $C^t_{eh}(r)$ (solid line), and exciton electron-hole correlation, $C^x_{ee}(r)$ (dashed-dotted line). The distances are in atomic units as defined in Sec. II F.

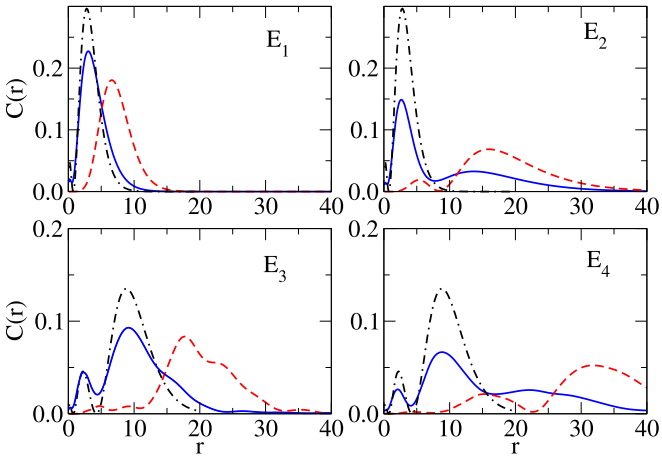

FIG. 5. Excited state correlation functions for $\tilde{r}_0 = 0$. Electron-electron correlation, $C^t_{ee}(r)$ (dashed line), electron-hole correlation, $C^t_{eh}(r)$ (solid line), and exciton electron-hole correlation, $C^x_{ee}(r)$ (dashed-dotted line). The distances are in atomic units as defined in Sec. II F.

away from the origin due to the repulsion. The structure of the trion is more or less similar to a system where an electron is orbiting around an exciton.

The exciton plus electron structure of the excited states shows a very similar tendency. Figure 5 shows the correlation functions for the four resonance states. E_1 and E_2 are below the $2s$ exciton threshold and they have a pronounced $2s$ exciton plus an outer electron structure. The electron-hole correlation function of the excited state trion is very similar to the electron-hole density in the exciton. The difference between the excited trion with energy E_1 and E_2 is that in the latter the second electron is much farther away from the exciton (as the electron-electron correlation function shows in Fig. 5). In the trion with energy E_2 the electron-hole correlation has a long tail overlapping with the electron electron-correlation function. The second electron strongly polarizes the exciton. The excited trion binding is due to the significant overlap between the electron-electron and electron-hole correlation functions. The excited states with energy E_3 and E_4 show a very similar tendency, an $3s$ exciton plus an electron far out from the center.

3. *Results for* $0 < \tilde{r}_0$

To calculate resonance states for $0 < \tilde{r}_0$ we use the ECG basis that is generated by SVM for $\tilde{r}_0 = 0$. The basis dimension is very large ($K = 1500$) and the basis is flexible enough to be accurate for nonzero $\tilde{r}_0$. Actually the $\tilde{r}_0 = 0$ case is the most challenging calculation because of the deep Coulomb potential near the origin. Increasing $\tilde{r}_0$ leads to less attractive potential close to the origin, while the asymptotic part ($r > 5$) of the potential still behaves like $1/r$. This asymptotic Coulomb part determines the resonance wave functions beyond $r = 5$ so one expects that the resonances also exist for $0 < \tilde{r}_0$.

Using the ECG basis optimized for $\tilde{r}_0 = 0$, we have diagonalized the Hamiltonian for different values of $\tilde{r}_0$. This step is an application of the SM approach to find resonance states by changing the potential strength. The calculated resonance energy, E_1, as a function $\tilde{r}_0$ is shown in Fig. 6. To check the SM approach we have also used the CS method. The ECG basis was optimized for several $\tilde{r}_0$ values and resonance positions were calculated by CS. These calculations have shown that resonance energy trajectory in Fig. 6 is accurate, and the CS also allowed us the determination of the resonance width (see Table I).

The calculated total energies and the binding energies for the ground state and the lowest two resonance states are shown in Figs. 7 and 8. We only show these two resonance states because the energy of the higher states barely depends on $\tilde{r}_0$ (see Table I). This is not surprising, the resonance states with

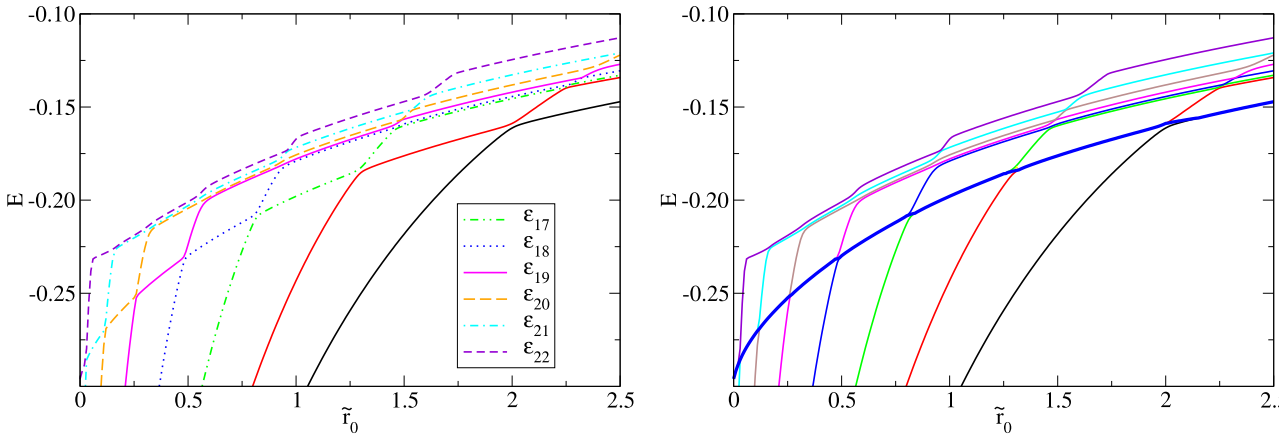

FIG. 6. Change of energy levels as a function of $\tilde{r}_0$. Left: By increasing $\tilde{r}_0$ the potential weakens and the energy levels move upward. The energy levels $\epsilon_{22}, \epsilon_{21}\ldots$ approximate the energy of the first resonance state E_1 at different values of $\tilde{r}_0$. At $\tilde{r} = 0$ the energy of the 22nd excited state ϵ_{22} approximates the excited trion state, E_1. By increasing $\tilde{r}_0$ ϵ_{22} moves upward, but at around $\tilde{r}_0 = 0.02$ the energy level ϵ_{21} moves up faster and becomes nearly equal to the energy level ϵ_{22}. The two energy levels cannot cross each other (avoided crossing) and E_1 will be approximated by ϵ_{21}. At $\tilde{r}_0 = 0.12$ ϵ_{20} approaches ϵ_{21} and E_1 will be approximated by ϵ_{20}. The next approximation will be ϵ_{19} and so on. Right: Same as in the left, but the complete trajectory of E_1 as a function of $\tilde{r}_0$ is highlighted (thick line). The energies and $\tilde{r}_0$ are in atomic units as defined in Sec. II F.

TABLE I. Energies and other properties of trion states for $S = 0$. For $\tilde{r}_0 = 0$ the ground state and five resonance states is shown. For $\tilde{r}_0 = 0.5$ and $\tilde{r}_0 = 1$ only four resonance state is listed because the energy of the 5th state is too close to the energy of the $3s$ exciton and the accurate calculation is very difficult.

$\tilde{r}_0$	E_r	E_i	r_{eh}	r_{eh}^2	δ_{eh}	r_{ee}	r_{ee}^2	δ_{ee}
	−2.2432	0	0.84	1.20	9.76	1.30	2.28	0.48
	−0.2832	-8.8×10^{-8}	4.09	20.93	0.22	7.38	59.98	9.52×10^{-5}
	−0.2267	-1.4×10^{-5}	9.98	171.58	0.26	18.98	414.41	2.37×10^{-5}
0	−0.1049	-1.7×10^{-4}	12.98	414.39	6.47×10^{-2}	24.07	957.33	1.92×10^{-4}
	−0.0886	-1.2×10^{-4}	16.88	421.15	3.90×10^{-2}	32.10	1179.79	4.52×10^{-4}
	−0.0814	-9.3×10^{-5}	29.82	1463.13	2.86×10^{-2}	57.80	3627.17	8.11×10^{-7}
	−0.8369	0	1.70	4.72	1.51	2.68	9.32	0.117
	−0.2217	-3.4×10^{-7}	5.42	42.86	7.36×10^{-2}	9.73	113.38	1.03×10^{-4}
0.5	−0.1926	-5.8×10^{-5}	29.06	1954.90	3.76×10^{-2}	55.01	3911.25	2.19×10^{-3}
	−0.0914	-1.6×10^{-4}	13.26	287.85	4.50×10^{-2}	24.17	720.18	1.25×10^{-3}
	−0.0781	-2.1×10^{-4}	27.74	1065.93	1.65×10^{-2}	43.59	2224.40	5.70×10^{-5}
	−0.5956	0	2.14	7.39	0.90	3.39	14.75	7.24×10^{-2}
	−0.1918	-2.2×10^{-7}	6.19	51.91	5.56×10^{-2}	11.08	138.89	5.29×10^{-2}
1	−0.1715	-6.7×10^{-5}	29.85	1960.28	5.23×10^{-3}	56.23	3922.15	3.84×10^{-2}
	−0.0841	-4.2×10^{-4}	18.16	829.50	4.34×10^{-2}	32.73	1809.85	1.93×10^{-3}
	−0.0740	-3.9×10^{-4}	25.11	1049.68	5.24×10^{-3}	45.55	2351.17	8.46×10^{-5}

higher energy only feel the $1/r$ tail of the potential, which is independent of $\tilde{r}_0$. The weak $\tilde{r}_0$ dependence is also true for the resonances with energy E_1 and E_2 above $\tilde{r}_0 = 1$. The mean distances between particles at $\tilde{r}_0 = 1$ are larger than $r = 5$ (see Table I) so these states are mostly affected by the Coulomb tail. Energies E_1 and E_2 proportional to the energy of the $2s$ trion (see Fig. 7) and the binding energy hardly changes (see Fig. 8).

The energies and the average distances between particles are compared in Table I for different $\tilde{r}_0$ values. Compared to the compact ground state trions, the electron-hole, and electron-electron distances are very large in the excited states. Table I also shows

$$\delta_{ee} = C_{ee}(0), \quad \text{and} \quad \delta_{eh} = C_{eh}(0), \tag{33}$$

the probability that the two electron or an electron and the hole are at the same spatial position. This probability is decreasing with the increased spatial distribution and the probability for electron-hole is always larger than that of the electron-electron.

The most interesting feature of the dependence of the binding energies on $\tilde{r}_0$ is that the excited states become more bound than the ground state by increasing $\tilde{r}_0$. The trajectory of E_1 and E_0 crosses at $\tilde{r}_0 = 0.55$ and E_2 and E_0 crosses at $\tilde{r}_0 = 1.4$. This happens because the ground state wave function (see Fig. 4) is nonzero close to the origin and increasing $\tilde{r}_0$ weakens the potential in that region and the ground state binding energy rapidly decreases with r_0 as Fig. 8 shows. As it was already mentioned, the excited states are mostly governed by the Coulomb tail and their energies are less sensitive to $\tilde{r}_0$.

The correlation functions of the excited states for $\tilde{r}_0 > 0$ is very similar to the $\tilde{r}_{=}0$ case shown in Fig. 5, but spatially more extended. This is because increasing $\tilde{r}_0$ the total energies are decreasing and the size of the states are increasing (see

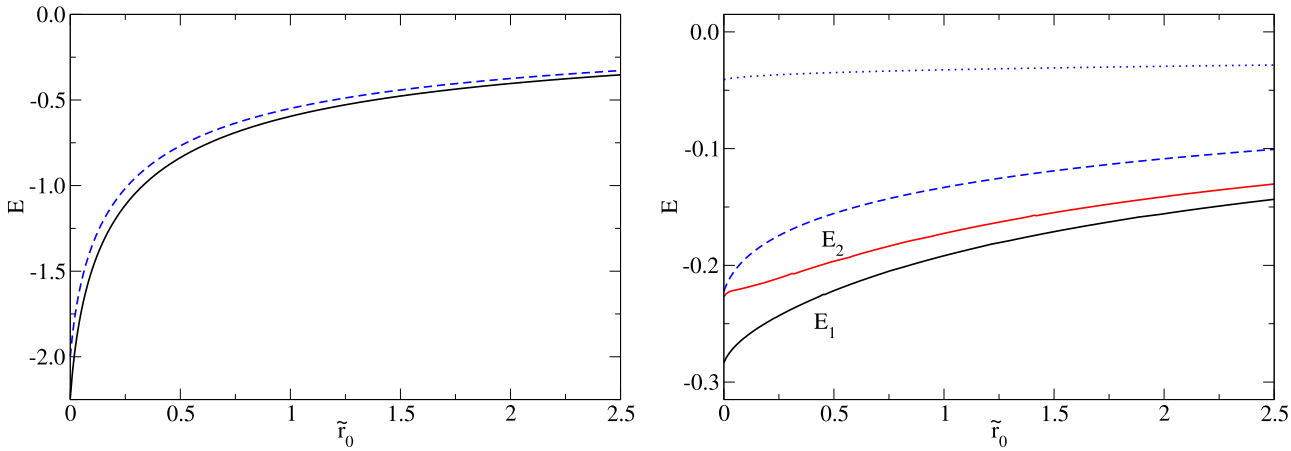

FIG. 7. Energies as a function of $\tilde{r}_0$. Left: Ground state energy trion, E_0 (solid line), $1s$ exciton energy (dashed line). Right: Excited state energies of trion, E_1 and E_2 (solid lines), $2s$ exciton energy (dashed line), $3s$ exciton energy (dotted line). The energies and $\tilde{r}_0$ are in atomic units as defined in Sec. II F.

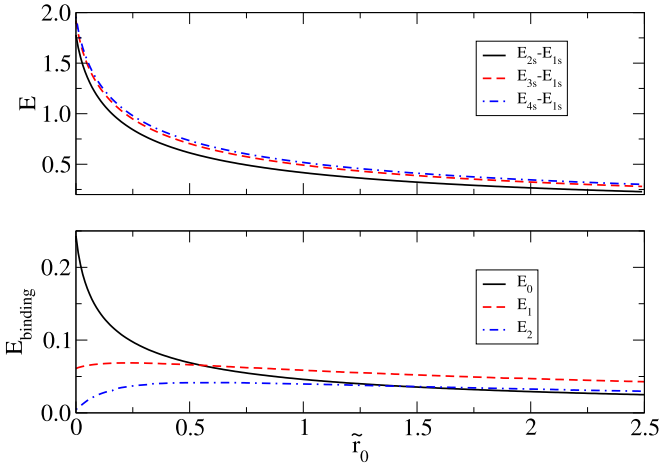

FIG. 8. Top: Transition energies of exciton excited states as a function of $\tilde{r}_0$. Bottom: Binding energies of the ground and the two lowest resonance states the ground and the two lowest resonance states as a function of $\tilde{r}_0$. The energies and $\tilde{r}_0$ are in atomic units as defined in Sec. II F.

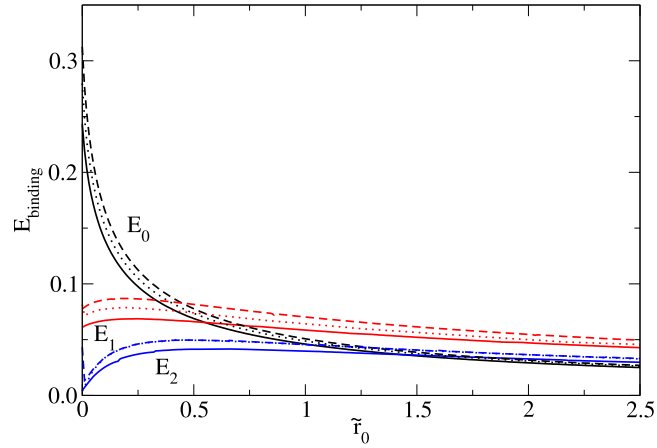

FIG. 9. Binding energies as a function of $\tilde{r}_0$ (solid line *eeh* with $\sigma = 1$, dotted line *eeh* with $\sigma = 2/3$, dashed line *ehh* with $\sigma = 2/3$. The energies and $\tilde{r}_0$ are in atomic units as defined in Sec. II F.

Table I). As an illustration for the similarity we show the ground state trion for $\tilde{r}_0 = 0$ and $\tilde{r}_0 = 1$ in Fig. 4.

We have also investigated the effect of electron and hole mass ratio on the binding energy. Due to the different masses the electron hole symmetry is broken so we have two different trions, *ehh* and *eeh*. To magnify the binding energy differences, we have used a relatively large hole mass by choosing $\sigma = 2/3$. For smaller hole masses the tendencies in the binding energies cannot be easily illustrated. Figure 9 shows the binding energy of *ehh* and *eeh* as a function of $\tilde{r}_0$. The heavier hole leads to larger binding energies compared to the $\sigma = 1$ case, and the *ehh* system is has larger binding energy than *eeh*, except for the E_2 resonance where the two energies are nearly equal. The mass difference also affects the crossing points.

B. Spin triplet case

Similarly to the 3D case [51], we have also found two resonances for spin triplet trions in 2D, one right below the $2s$ threshold and one very close to the $3s$ threshold, so the binding energies of these resonances is very small (see Table II). The average distances in these systems are very similar to the those of the singlet E_1 and E_3, respectively.

Figure 10 compares the correlation function of the exciton and the triplet trion resonances. Once again, the electron-hole correlation function is very similar to the $2s$ and $3s$ exciton. The peak of electron-electron correlation function, however, is almost twice as far away then in the singlet case (see Fig. 5 E_1 and E_3) because the two electron has parallel spins.

C. Comparison to experiments

In this section, we compare the calculated results to experimental measurements in monolayer TMDs sandwiched between hexagonal boron nitride. The encapsulation of TMD monolayers between atomically smooth hexagonal boron nitride layers allows high quality optical measurements. Binding energies and radii of Rydberg exciton states and energies of charged excitons were measured in WS_2 [2,11], WSe_2 [5,19,44,71–73], MoS_2 [1,7,74–76], $MoSe_2$ [75,77] and $MoTe_2$ [75,77].

Using the parameters (μ, r_0, and κ) given in Table I of Ref. [75] we have calculated the binding energies and root mean square distances of excitons and trions in WS_2, WSe_2, $MoSe_2$, MoS_2, and $MoTe_2$ (Table III). Note, that in some cases the $\tilde{r}_0$ values are very different, but the energies are very similar. For example, the binding energies of WS_2 and WSe_2 are very close despite the difference in $\tilde{r}_0$. This is because of the change of binding energy between $\tilde{r}_0 = 0.59$ and $\tilde{r}_0 = 0.84$ is compensated by the slightly larger E^* of WSe_2. E^* is inversely proportional to κ^2 so small changes in κ can cause large energy changes.

The calculated binding energies and radii for excitons (Table III) are in excellent agreement with the experimental binding energy and radii of Table I of Ref. [75], reproducing the fit of the model to experimental data of Ref. [75]. The calculated exciton radii and energies are also in agreement with the calculated and the experimental values for WSe_2 [6] (the calculated $r_{eh}^2 = 1.67$ nm for $1s$ and $r_{eh}^2 = 6.96$ nm for $2s$, the experimental values are 1.7 and 6.6 nm, the calculated $E_{2s} - E_{1s}$ is 124 meV, and the experimental value is 130 meV).

In previous calculations (see Table II of Ref. [31]) for TMDs suspended in vacuum or placed on SiO_2 substrate

TABLE II. Energies and other properties of trion states for $S = 1$, $\tilde{r}_0 = 0$ and $\sigma = 1$.

E_r	E_i	r_{eh}	r_{eh}^2	δ_{eh}	r_{ee}	r_{ee}^2	δ_{ee}
-0.2254	-5.0×10^{-6}	11.94	256.66	0.16	22.88	599.55	1.5×10^{-12}
-0.0845	-1.2×10^{-6}	19.61	573.79	0.03	37.72	1568.04	1.9×10^{-11}

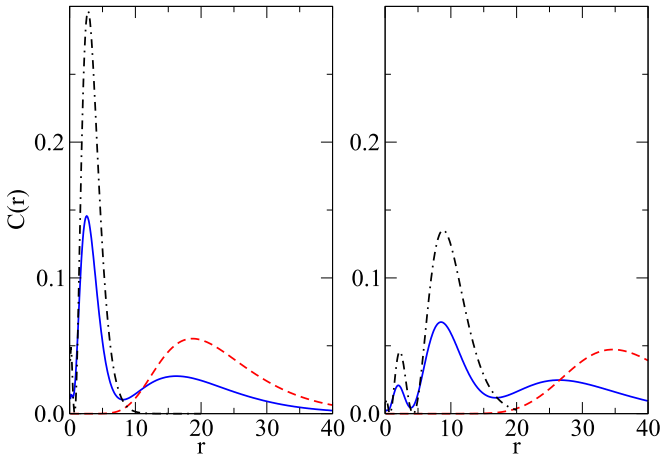

FIG. 10. Ground state correlation functions for $S = 1$ resonances below the $2s$ threshold (left) and below the $3s$ threshold (right). Electron-electron correlation, $C^t_{ee}(r)$ (dashed line), electron-hole correlation, $C^t_{eh}(r)$ (solid line), and exciton electron-hole correlation, $C^x_{ee}(r)$ (dashed-dotted line for $2s$ exciton (left) and $3s$ exciton (right). The distances are in atomic units as defined in Sec. II F.

the calculated and experimental energies of excitons were 50–100 meV different. The more accurate measurements using monolayer TMDs sandwiched between hexagonal boron nitride layers allow the study of the Rydberg states of excitons in a magnetic field and one can extract the binding energy and radii of the Rydberg states [75]. These physical properties then can be used to find the most suitable model parameters, reducing the difference between the experimental and theoretical binding energy of excitons to less than 5 meV.

The agreement of calculated and experimental binding energies (Table III) is not as good as for excitons, but in general it is similar to the agreement for the TMDs suspended in vacuum or placed on SiO_2 surface [31,35]. Comparing the experimental and calculated trion energies one has to keep in mind that the model parameters were fitted to the exciton measurements [75], but the trion energies were not measured in the same experiment. For example, the $E_{2s} - E_{1s}$ energy difference was measured to be 141.7 meV for WS_2 in Ref. [75]. The value of this transition energy is very important to find the screening length. In Ref. [11] trion states at 31 and 37 meV were reported in WS_2, but the $E_{2s} - E_{1s}$ difference was measured to be 145 meV in this experiment. This small

TABLE III. Energies and mean distances in TMDs. Energies are in meV, distances and in nm, $E^b_1 = E_1 - E_{1s}$, $E^b_2 = E_2 - E_{2s}$, $E^b_3 = E_3 - E_{2s}$.

System	Property	Method	WS_2	WSe_2	MoS_2	$MoSe_2$	$MoTe_2$
	$\tilde{r}_0$		0.5942	0.8399	0.8923	1.3324	2.2489
	E_{1s}	Calc	−178.7	−161.4	−220.2	−231.9	−176.9
	E_{1s}	Exp	−180[a]	−167[a], −170[h]	−221[a,i]	−231[a]	−177[a]
	$\sqrt{\langle r^2_{eh}\rangle}$	Calc	1.66	1.68	1.23	1.10	1.31
eh	$\sqrt{\langle r^2_{eh}\rangle}$	Exp	1.8[a]	1.7[a,b]	1.2[a]	1.1[a]	1.3[a]
	E_{2s}	Calc	−37.8	−37.4	−51.8	−60.6	−52.8
	$\sqrt{\langle r^2_{eh}\rangle}$	Calc	7.20	6.97	5.08	4.32	4.81
	$\sqrt{\langle r^2_{eh}\rangle}$	Exp		6.6[a]			
	$E_{2s} - E_{1s}$	Calc	140.9	124	168.4	171.3	124.1
	$E_{2s} - E_{1s}$	Exp	141.7[a]	130[b],131[h]	170[a,i]	168[a], 148[j], 152[c]	124[a,j]
	E_0	Calc	−194.4	−175.2	−238.8	−250.8	−190.5
	E_0[b]	Calc	15.7	13.8	16.6	18.9	13.6
	E_0[b]	Exp	27, 31[d]	21,29[e]	17, 25[f]	27[c,g]	
	$\sqrt{\langle r^2_{eh}\rangle}$	Calc	3.01	3.05	2.2	2.0	2.4
	$\sqrt{\langle r^2_{ee}\rangle}$	Calc	4.24	4.03	3.2	2.8	3.4
	E_1	Calc	−54.1	−53.8	−74.4	−87.3	−75.5
	E_1[b]	Calc	16.3	16.4	22.6	26.6	22.7
eeh	E_1[b]	Exp	22[d]			27[c]	
	$\sqrt{\langle r^2_{eh}\rangle}$	Calc	8.5	8.83	6.1	5.5	5.8
	$\sqrt{\langle r^2_{ee}\rangle}$	Calc	13.9	14.20	9.9	8.8	9.4
	E_2	Calc	−48.0	−48.1	−66.8	−78.8	−67.9
	E_2[b]	Calc	10.2	10.7	15.1	18.2	15.1
	$\sqrt{\langle r^2_{eh}\rangle}$	Calc	54.9	45.8	29.0	28.2	29.3
	$\sqrt{\langle r^2_{ee}\rangle}$	Calc	77.6	64.9	41.1	40.0	41.4

[a][75]; [b][6]; [c][45]; [d][11]; [e][17]; [f][74]; [g][72]; [h][78]; [i][76]; [j][77].

difference (141.7 meV to fit the parameter and 145 meV in the measurement) would lead to a relatively large change in the model parameters and would affect the binding energy of the trions. Another factor to consider is the effective mass, μ. The energy of the exciton only depends on μ so the experiments can only pinpoint the reduced mass but give no guidance about the effective mass of the hole. In the calculations presented in Table III we used $m_e = m_h$ ($\sigma = 1$). As it is illustrated in Fig. 9, using different values for the electron and hole mass while keeping the reduced mass the same increases the binding energies. For the energy of trions in TMDs (see Table III) this would lead to a 3–5 meV increase in binding energies.

The calculated binding energy for the excited-state trions is about the same range as the ground state binding energies, these excited states have relatively large binding energies. An excited-state trion was recently reported in WS_2 [11] and $MoSe_2$ [45] with binding energies close to the binding energy of the ground state. The width of these resonance states is very small and these are quasi-bound states. In the lower excited state, E_1, the *eh* and *ee* distance about 2.5 to 3 times larger than in the ground state. This state is a $2s$ exciton with a loosely bound electron (or hole) circling around it. The second excited state, E_2, is even larger with tens of nanometers of distances between *ee* and *eh*. Due to the large size, this state is a model prediction in a perfect 2D system, but it is unlikely that this can be measured in a real material.

Figure 8 can be used as a guide to analyzing the agreement between the Keldysh potential based models and experiments. If the energy differences between the Rydberg exciton states are measured, one can choose the most suitable $\tilde{r}_0$ value using the top part of Fig. 8. This value then can be used to predict the trion energies using the bottom part of Fig. 8.

IV. SUMMARY

Using the complex scaling and the stabilization method combined with the stochastic variational approach, we have studied resonance states of three-particle systems interacting with a Coulomb and a screened Coulomb (Keldysh potential). The stochastic variational method was used to generate a suitable square integrable basis of explicitly correlated Gaussians. The stochastic variational method has been previously used [31,35] to describe trions, biexcitons, and charged biexcitons in TMDs and in high precision calculations in atomic and molecular systems [46]. We have used two independent approaches, the CS, and the stabilization to calculate the resonance states using real basis functions.

In 2D Coulomb three-particle systems with $S = 0$, we have found three resonance states below the $2s$ and two resonance states below the $3s$ two-particle (exciton) threshold. These states can be envisioned as a $2s$ or $3s$ exciton with a third, loosely bound particle circling around it. Comparing the correlation functions of $2s$ and $3s$ excitons to those of the excited trions confirm that picture. We have also found two resonance states for $S = 1$. Resonance states similar to these have been studied in 3D for Coulomb potential [51]. These resonances are mostly due to the long tail of the Coulomb interaction and they survive the confinement from 3D to 2D, despite the fact that their energy and spatial extension radically changes.

Screening the Coulomb interaction using a Keldysh potential changes the energy of these resonances, but they remain narrow quasibound states. The screening decreases the Coulomb potential at the origin, pushing the resonance wave function farther out, so the interparticle distances quickly increase. As the wave functions of the resonance states are mostly feeling the Coulomb tail, the resonance energies are less sensitive to the screening than the energy of the ground state. At some screening length, the binding energy of the resonance states will be larger than that of the ground state.

We have calculated the energies and interparticle distances of these resonance states for various TMDs. Energies of excited-state trions in WS_2 [11] and $MoSe_2$ [45] are reasonably close to the values predicted by the calculations. A closer agreement may require more elaborate calculations including spin-orbit interactions and multiband Hamiltonians as used, for example, in Ref. [35].

ACKNOWLEDGMENTS

K.V. was supported by the National Science Foundation (NSF) under Grant No. IRES 1826917, J.Y. acknowledges support from NSF Grant No. ECCS-1509599.

[1] K. F. Mak, C. Lee, J. Hone, J. Shan, and T. F. Heinz, Phys. Rev. Lett. **105**, 136805 (2010).
[2] A. Chernikov, T. C. Berkelbach, H. M. Hill, A. Rigosi, Y. Li, O. B. Aslan, D. R. Reichman, M. S. Hybertsen, and T. F. Heinz, Phys. Rev. Lett. **113**, 076802 (2014).
[3] M. M. Ugeda, A. J. Bradley, S.-F. Shi, F. H. da Jornada, Y. Zhang, D. Y. Qiu, W. Ruan, S.-K. Mo, Z. Hussain, Z.-X. Shen, F. Wang, S. G. Louie, and M. F. Crommie, Nat. Mater. **13**, 1091 (2014).
[4] Z. Ye, T. Cao, K. O'Brien, H. Zhu, X. Yin, Y. Wang, S. G. Louie, and X. Zhang, Nature (London) **513**, 214 (2014).
[5] K. He, N. Kumar, L. Zhao, Z. Wang, K. F. Mak, H. Zhao, and J. Shan, Phys. Rev. Lett. **113**, 026803 (2014).
[6] A. V. Stier, N. P. Wilson, K. A. Velizhanin, J. Kono, X. Xu, and S. A. Crooker, Phys. Rev. Lett. **120**, 057405 (2018).
[7] K. F. Mak, K. He, C. Lee, G. H. Lee, J. Hone, T. F. Heinz, and J. Shan, Nat. Mater. **12**, 207 (2013).
[8] B. Zhu, H. Zeng, J. Dai, Z. Gong, and X. Cui, Proc. Natl. Acad. Sci. USA **111**, 11606 (2014).
[9] G. Wang, L. Bouet, D. Lagarde, M. Vidal, A. Balocchi, T. Amand, X. Marie, and B. Urbaszek, Phys. Rev. B **90**, 075413 (2014).
[10] C. Zhang, H. Wang, W. Chan, C. Manolatou, and F. Rana, Phys. Rev. B **89**, 205436 (2014).
[11] A. Arora, T. Deilmann, T. Reichenauer, J. Kern, S. Michaelis de Vasconcellos, M. Rohlfing, and R. Bratschitsch, Phys. Rev. Lett. **123**, 167401 (2019).

[12] Y. You, X.-X. Zhang, T. C. Berkelbach, M. S. Hybertsen, D. R. Reichman, and T. F. Heinz, Nat. Phys. **11**, 477 (2015).

[13] G. Plechinger, P. Nagler, J. Kraus, N. Paradiso, C. Strunk, C. Schüller, and T. Korn, Phys. Status Solidi RRL **9**, 457 (2015).

[14] Y. Meng, T. Wang, Z. Li, Y. Qin, Z. Lian, Y. Chen, M. C. Lucking, K. Beach, T. Taniguchi, K. Watanabe, S. Tongay, F. Song, H. Terrones, and S.-F. Shi, Nano Lett. **19**, 299 (2019).

[15] C. E. Stevens, J. Paul, T. Cox, P. K. Sahoo, H. R. Gutiérrez, V. Turkowski, D. Semenov, S. A. McGill, M. D. Kapetanakis, I. E. Perakis, D. J. Hilton, and D. Karaiskaj, Nat. Commun. **9**, 3720 (2018).

[16] M. Barbone, A. R. P. Montblanch, D. M. Kara, C. Palacios-Berraquero, A. R. Cadore, D. De Fazio, B. Pingault, E. Mostaani, H. Li, B. Chen, K. Watanabe, T. Taniguchi, S. Tongay, G. Wang, A. C. Ferrari, and M. Atatüre, Nat. Commun. **9**, 3721 (2018).

[17] S.-Y. Chen, T. Goldstein, T. Taniguchi, K. Watanabe, and J. Yan, Nat. Commun. **9**, 3717 (2018).

[18] Z. Li, T. Wang, Z. Lu, C. Jin, Y. Chen, Y. Meng, Z. Lian, T. Taniguchi, K. Watanabe, S. Zhang, D. Smirnov, and S.-F. Shi, Nat. Commun. **9**, 3719 (2018).

[19] Z. Ye, L. Waldecker, E. Y. Ma, D. Rhodes, A. Antony, B. Kim, X.-X. Zhang, M. Deng, Y. Jiang, Z. Lu, D. Smirnov, K. Watanabe, T. Taniguchi, J. Hone, and T. F. Heinz, Nat. Commun. **9**, 3718 (2018).

[20] M. He, P. Rivera, D. Van Tuan, N. P. Wilson, M. Yang, T. Taniguchi, K. Watanabe, J. Yan, D. G. Mandrus, H. Yu, H. Dery, W. Yao, and X. Xu, Nat. Commun. **11**, 618 (2020).

[21] W. Wang, N. Sui, M. Ni, X. Chi, L. Pan, H. Zhang, Z. Kang, Q. Zhou, and Y. Wang, J. Phys. Chem. C **124**, 1749 (2020).

[22] I. Kylänpää and H.-P. Komsa, Phys. Rev. B **92**, 205418 (2015).

[23] T. C. Berkelbach, M. S. Hybertsen, and D. R. Reichman, Phys. Rev. B **88**, 045318 (2013).

[24] G. Berghäuser and E. Malic, Phys. Rev. B **89**, 125309 (2014).

[25] P. Cudazzo, I. V. Tokatly, and A. Rubio, Phys. Rev. B **84**, 085406 (2011).

[26] M. Bieniek, L. Szulakowska, and P. Hawrylak, Phys. Rev. B **101**, 125423 (2020).

[27] B. Ganchev, N. Drummond, I. Aleiner, and V. Fal'ko, Phys. Rev. Lett. **114**, 107401 (2015).

[28] M. Z. Mayers, T. C. Berkelbach, M. S. Hybertsen, and D. R. Reichman, Phys. Rev. B **92**, 161404(R) (2015).

[29] K. A. Velizhanin and A. Saxena, Phys. Rev. B **92**, 195305 (2015).

[30] D. K. Zhang, D. W. Kidd, and K. Varga, Nano Lett. **15**, 7002 (2015).

[31] D. W. Kidd, D. K. Zhang, and K. Varga, Phys. Rev. B **93**, 125423 (2016).

[32] E. Prada, J. V. Alvarez, K. L. Narasimha-Acharya, F. J. Bailen, and J. J. Palacios, Phys. Rev. B **91**, 245421 (2015).

[33] S. C. Kuhn and M. Richter, Phys. Rev. B **101**, 075302 (2020).

[34] S. C. Kuhn and M. Richter, Phys. Rev. B **99**, 241301(R) (2019).

[35] M. Van der Donck, M. Zarenia, and F. M. Peeters, Phys. Rev. B **96**, 035131 (2017).

[36] D. Van Tuan, B. Scharf, Z. Wang, J. Shan, K. F. Mak, I. Žutić, and H. Dery, Phys. Rev. B **99**, 085301 (2019).

[37] E. Mostaani, M. Szyniszewski, C. H. Price, R. Maezono, M. Danovich, R. J. Hunt, N. D. Drummond, and V. I. Fal'ko, Phys. Rev. B **96**, 075431 (2017).

[38] D. K. Efimkin and A. H. MacDonald, Phys. Rev. B **95**, 035417 (2017).

[39] S. Wu, L. Cheng, and Q. Wang, Phys. Rev. B **100**, 115430 (2019).

[40] C. Fey, P. Schmelcher, A. Imamoglu, and R. Schmidt, Phys. Rev. B **101**, 195417 (2020).

[41] T. Deilmann and K. S. Thygesen, Phys. Rev. B **96**, 201113(R) (2017).

[42] R. Y. Kezerashvili, Few-Body Syst. **60**, 52 (2019).

[43] M. Van der Donck, M. Zarenia, and F. M. Peeters, Phys. Rev. B **97**, 195408 (2018).

[44] E. Courtade, M. Semina, M. Manca, M. M. Glazov, C. Robert, F. Cadiz, G. Wang, T. Taniguchi, K. Watanabe, M. Pierre, W. Escoffier, E. L. Ivchenko, P. Renucci, X. Marie, T. Amand, and B. Urbaszek, Phys. Rev. B **96**, 085302 (2017).

[45] T. Goldstein, Y.-C. Wu, S.-Y. Chen, T. Taniguchi, K. Watanabe, K. Varga, and J. Yan, arXiv:2005.05829.

[46] J. Mitroy, S. Bubin, W. Horiuchi, Y. Suzuki, L. Adamowicz, W. Cencek, K. Szalewicz, J. Komasa, D. Blume, and K. Varga, Rev. Mod. Phys. **85**, 693 (2013).

[47] J. Usukura, Y. Suzuki, and K. Varga, Phys. Rev. B **59**, 5652 (1999).

[48] K. Varga, Phys. Rev. Lett. **83**, 5471 (1999).

[49] C. Riva, F. M. Peeters, and K. Varga, Phys. Rev. B **61**, 13873 (2000).

[50] Y. K. Ho, Phys. Rev. A **19**, 2347 (1979).

[51] J. Usukura and Y. Suzuki, Phys. Rev. A **66**, 010502(R) (2002).

[52] J. Z. Mezei, A. T. Kruppa, and K. Varga, Few-Body Syst. **41**, 233 (2007).

[53] A. U. Hazi and H. S. Taylor, Phys. Rev. A **1**, 1109 (1970).

[54] Y. Ho, Phys. Rep. **99**, 1 (1983).

[55] N. Moiseyev, Phys. Rep. **302**, 212 (1998).

[56] Y. Suzuki and K. Varga, *Stochastic Variational Approach to Quantum-Mechanical Few-Body Problems* (Springer, Berlin, 1998).

[57] J. Usukura, K. Varga, and Y. Suzuki, Phys. Rev. A **58**, 1918 (1998).

[58] L. V. Keldysh, JETP Lett. **29**, 658 (1979).

[59] D. Van Tuan, M. Yang, and H. Dery, Phys. Rev. B **98**, 125308 (2018).

[60] R. Krivec, V. B. Mandelzweig, and K. Varga, Phys. Rev. A **61**, 062503 (2000).

[61] J. Aguilar and J. M. Combes, Commun. Math. Phys. **22**, 269 (1971).

[62] E. Balslev and J. M. Combes, Commun. Math. Phys. **22**, 280 (1971).

[63] E. A. Hylleraas and B. Undheim, Z. Phys. **65**, 759 (1930).

[64] J. K. L. MacDonald, Phys. Rev. **43**, 830 (1933).

[65] F. M. Pont, P. Serra, and O. Osenda, J. Phys. B **44**, 135003 (2011).

[66] Y. Sajeev, Chem. Phys. Lett. **587**, 105 (2013).

[67] T. C. Thompson and D. G. Truhlar, Chem. Phys. Lett. **92**, 71 (1982).

[68] A. Macías and A. Riera, Chem. Phys. Lett. **164**, 359 (1989).

[69] P.-O. Löwdin, Int. J. Quantum Chem. **27**, 495 (1985).

[70] X. L. Yang, S. H. Guo, F. T. Chan, K. W. Wong, and W. Y. Ching, Phys. Rev. A **43**, 1186 (1991).

[71] T. P. Lyons, S. Dufferwiel, M. Brooks, F. Withers, T. Taniguchi, K. Watanabe, K. S. Novoselov, G. Burkard, and A. I. Tartakovskii, Nat. Commun. **10**, 2330 (2019).

[72] E. Liu, J. van Baren, Z. Lu, M. M. Altaiary, T. Taniguchi, K. Watanabe, D. Smirnov, and C. H. Lui, Phys. Rev. Lett. **123**, 027401 (2019).

[73] A. M. Jones, H. Yu, J. R. Schaibley, J. Yan, D. G. Mandrus, T. Taniguchi, K. Watanabe, H. Dery, W. Yao, and X. Xu, Nat. Phys. **12**, 323 (2016).

[74] J. G. Roch, G. Froehlicher, N. Leisgang, P. Makk, K. Watanabe, T. Taniguchi, and R. J. Warburton, Nat. Nanotechnol. **14**, 432 (2019).

[75] M. Goryca, J. Li, A. V. Stier, T. Taniguchi, K. Watanabe, E. Courtade, S. Shree, C. Robert, B. Urbaszek, X. Marie, and S. A. Crooker, Nat. Commun. **10**, 4172 (2019).

[76] C. Robert, M. A. Semina, F. Cadiz, M. Manca, E. Courtade, T. Taniguchi, K. Watanabe, H. Cai, S. Tongay, B. Lassagne, P. Renucci, T. Amand, X. Marie, M. M. Glazov, and B. Urbaszek, Phys. Rev. Mater. **2**, 011001 (2018).

[77] B. Han, C. Robert, E. Courtade, M. Manca, S. Shree, T. Amand, P. Renucci, T. Taniguchi, K. Watanabe, X. Marie, L. E. Golub, M. M. Glazov, and B. Urbaszek, Phys. Rev. X **8**, 031073 (2018).

[78] S.-Y. Chen, Z. Lu, T. Goldstein, J. Tong, A. Chaves, J. Kunstmann, L. S. R. Cavalcante, T. Woźniak, G. Seifert, D. R. Reichman, T. Taniguchi, K. Watanabe, D. Smirnov, and J. Yan, Nano Lett. **19**, 2464 (2019).